JOINT INVERSION OF TEMPERATURES IN A SYNTHETIC GEOTHERMAL FIELD USING MT, CLAY ALTERATION MODELS, AND GEOTHERMAL RESERVOIR SIMULATION

David Dempsey[1], John O'Sullivan[1], Sophie Pearson[2]

[1]University of Auckland, Auckland, New Zealand

[2]GNS Science, Upper Hutt, New Zealand

d.dempsey@auckland.ac.nz

Keywords: *Joint inversion, magneto-telluric, clay alteration, resistivity, geothermal reservoir simulation.*

ABSTRACT

Joint inversion seeks to assimilate multiple data streams with the goal of constraining the spatial distribution of some subsurface quantity. In this paper, we demonstrate a joint inversion approach that utilizes magneto-telluric (MT) survey data and a downhole temperature profile to infer the subsurface temperature distribution in a geothermal system. Specifically, we focus on interpreting the low resistivity anomaly associated with a hydrothermally altered clay clap, which, given an understanding of the clay formation temperature range, carries information about the contemporary temperature field.

The workflow we develop here involves: (i) simulating natural-state temperatures in a geothermal system, (ii) a model for hydrothermal alteration, (iii) forward simulation and (iv) subsequent inversion of MT surface observations, (v) modelling of collocated resistivity and downhole temperature profiles, which is then (vi) extrapolated to obtain an inferred temperature distribution away from the borehole. The workflow is demonstrated for the synthetic test case of a simple geothermal system. Inferred temperatures resulting from the joint inversion agree well with the true values in the vicinity of the clay cap but worsen rapidly outside the lateral extent of this region.

1. INTRODUCTION

A major challenge associated with geothermal exploration and field operation is a lack of information about conditions below ground. Wellbore surveys provide information about the system along a particular well track, but this understanding is difficult to extrapolate away from the borehole. In contrast, geophysical techniques based on inverse modelling, e.g., magneto-tellurics (MT), seismic tomography, provide constraint on rock property variation in the subsurface volume. While these properties (resistivity, seismic velocity) are not directly useful in modelling heat and mass flow in the reservoir, they can indicate features of interest, e.g., a low electrical resistivity anomaly could indicate a zone of clay alteration and the attendant formation temperatures and low permeability cap structure.

The goal of joint inversion is to integrate direct borehole measurements with indirect geophysical observations to obtain a better understanding of a quantity of interest. For

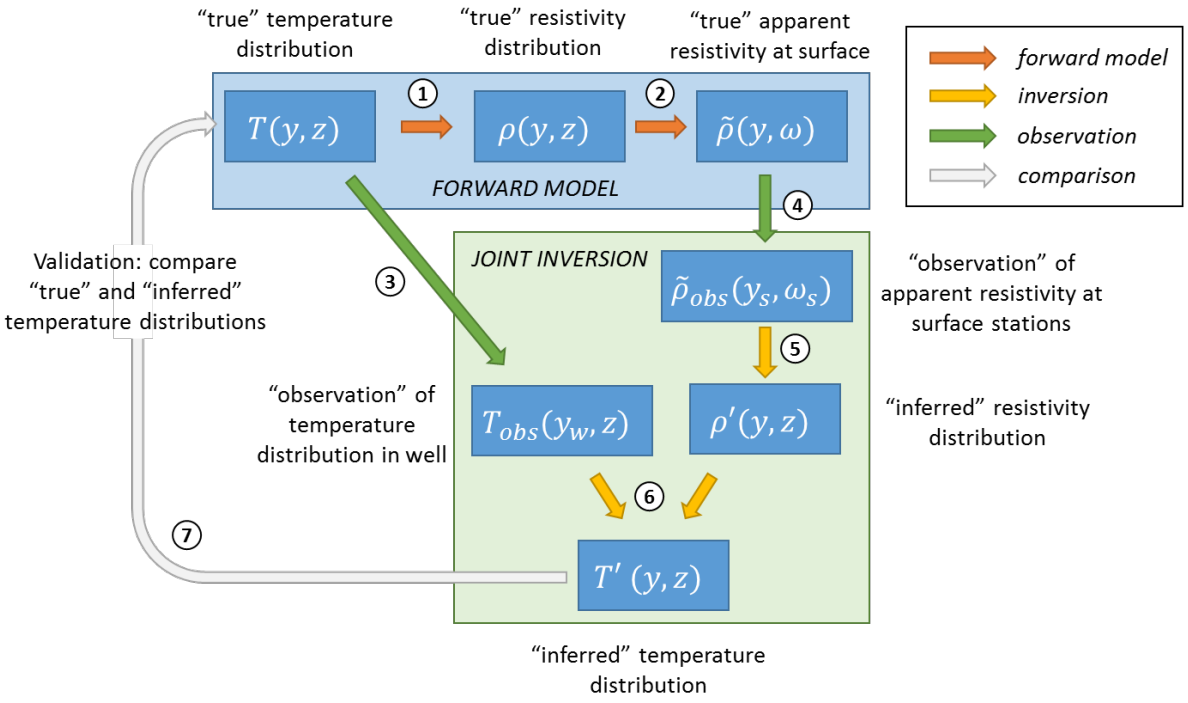

Figure 1: Schematic outlining the main steps in joint inversion of a 2D synthetic temperature distribution. Numbered steps are referred to in the text. T = temperature, ρ = electrical resistivity, $\tilde{\rho}$ = apparent resistivity, ω = frequency, y_w = horizontal well location, subscript s indicates an MT surface station (position and frequency), subscript obs indicates an observation and primed variables are inferred distributions.

instance, Mellors et al. (2015) describe a stochastic joint inversion approach that integrates wellbore temperature profiles with resistivity measurements from an MT survey to estimate the geometry and permeability of subsurface features. Muñoz et al. (2010) analysed co-located distributions of resistivity and seismic velocity (obtained from MT inversion and seismic tomography, respectively) for correlation structures. They identified five distinct clusters that were subsequently mapped onto a geological model for interpretation.

In this study, we develop a joint inversion methodology that focuses on interpretation of the low resistivity anomaly overlying a geothermal system revealed by an MT survey. Typically, this anomaly indicates the presence of conductive smectite clays that form by hydrothermal alteration within a particular band of temperatures. The resistivity anomaly is correlated to temperature data from an intersecting geothermal well, which enables extrapolation of temperature away from the borehole.

The proposed joint inversion workflow is demonstrated for a synthetic geothermal field as follows (Fig.1). First, a natural-state temperature distribution is simulated for a simple geothermal system. These temperatures inform a simple hydrothermal alteration model that delineates regions of low electrical resistivity (associated with clay formation) superimposed on a background resistivity model appropriate for the Taupo Volcanic Zone (TVZ), New Zealand. An MT simulation code is then used to convert the subsurface resistivity distribution to an apparent resistivity that would be measured by MT stations at the surface. These components comprise the *forward model*, which is then sampled to obtain synthetic observations. Joint inversion of the synthetic observations involves, first, inversion of the MT survey data to infer the subsurface resistivity distribution, followed by correlation to the wellbore temperature measurements and extrapolation away from the borehole. The approach is validated by comparing the known (steady-state model) and inferred temperature distributions.

2. FORWARD MODEL DESCRIPTION

The role of the forward model is to generate a synthetic MT signal that would be sampled by stations at the Earth's surface. The three steps are:

1. Simulate the static temperature distribution associated with a geothermal system at natural state.
2. Model alteration and resistivity changes as a simple function of rock temperature.
3. Simulate apparent resistivity at surface stations above the geothermal field.

Each of these model components is expanded on below.

2.1 Geothermal temperature distribution

Heat and mass transport within a convecting hydrothermal cell are simulated using AUTOUGH2 with the air-water equation of state. In this paper, we consider a simple representation of a geothermal system, comprising a single upflow zone situated beneath a topographic high (Fig. 2A).

The 1/4 symmetry model grid extends to 3 km depth and 10 km in each of the horizontal directions. The highest resolution is at the surface and at the corner at which the upflow is centred.

Because the convection cell is truncated at a depth of 3 km, it is necessary to inject mass at the bottom boundary (Fig. 2B). The symmetry boundaries are closed to heat and mass flow, while the exterior boundaries permit cold recharge at fixed pressure. A rainfall recharge boundary condition applied at the surface results in natural evolution of the water table. Further details about the model can be found in O'Sullivan and O'Sullivan (2016).

A natural state temperature distribution is obtained by running the model from a cold initial condition until pressures and temperatures are no longer changing. For the rest of the analysis we use the steady-state temperatures for a slice along the $\boldsymbol{y}$-axis, $\boldsymbol{T}(\boldsymbol{y},\boldsymbol{z})$, as shown in Fig. 2A.

In spite only existing within a synthetic model, we refer to $\boldsymbol{T}$ as the "true" temperature distribution. An observer standing at the Earth's surface has only limited information about $\boldsymbol{T}$. Just as with temperatures in a real geothermal system, they could gain some understanding of $\boldsymbol{T}$ by sampling at the location of wells. The goal of joint inversion is to complement these downhole measurements with an MT inversion, thereby inferring how $\boldsymbol{T}$ behaves away from the boreholes.

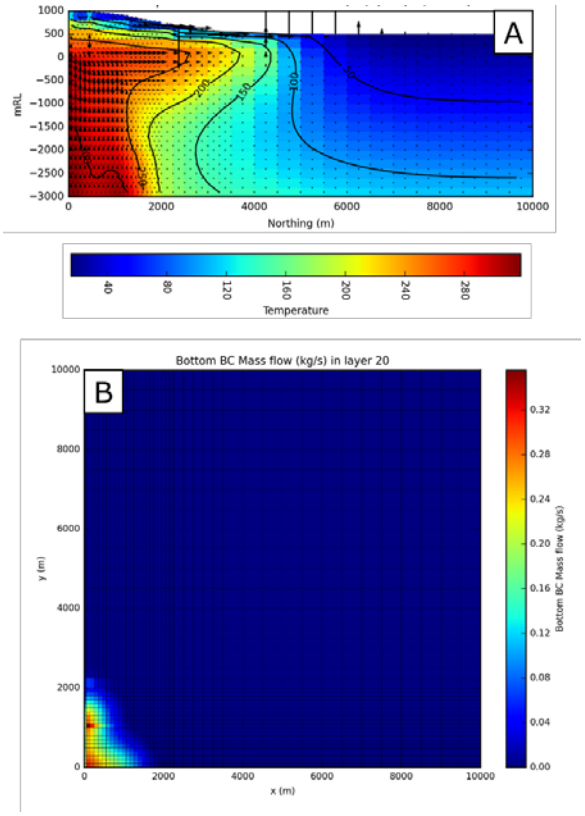

Figure 2: Summary of geothermal model. A. "True" temperature distribution, $\boldsymbol{T}(\boldsymbol{y},\boldsymbol{z})$. Black contours are isotherms and arrows show direction and size of mass flux. B. Mass flux boundary condition at the bottom of the model.

2.2 Alteration and resistivity change

We adopt a simple clay alteration model that computes the resistivity of altered rock as a function of temperature only. In practice, altered resistivity may also depend on rock lithology, fluid chemistry and degree of equilibration.

The model takes the form of a smoothed boxcar function, denoted $\Gamma(\cdot)$, whose shape is determined by six parameters:

- T_m, the temperature at the centre of the boxcar.
- T_w, the width of the boxcar.
- T_{wl}, the width of the lefthand transition zone.
- T_{wr}, the width of the righthand transition zone.
- ρ_a, the altered resistivity.
- ρ_0, the background resistivity.

By modifying these six parameters, a wide range of thermal alteration models can be considered. For a particular choice of parameters, $\boldsymbol{\theta} = [T_m, T_w, T_{wl}, T_{wr}, \rho_a, \rho_0]$, and the 2D temperature distribution from the geothermal model, we obtain a 2D resistivity distribution, $\rho(y,z) = \Gamma(T(y,z); \boldsymbol{\theta})$. Just as we referred to T as the "true" temperature distribution, we denote ρ the "true" resistivity distribution.

Fig. 3A shows the resistivity model for one particular parameter set: T_m = 200°C, T_w = 40°C, T_{wl} = T_{wr} = 10°C, ρ_a = 10 Ωm, and ρ_0 = 200 Ωm. This selection is based on a review of the available literature (Morrison, 1997), although other choices may be equally good or better for a particular field. For these parameters, Fig. 3B shows the 2D resistivity distribution corresponding to the temperatures in Fig. 2B.

Application of the alteration model corresponds to the arrow labeled ① in Fig. 1.

2.3 Apparent resistivity at surface

The MT analysis is simplified by considering only a 2D Earth, in which case there are two independent components of apparent resistivity. In future, it will be important to consider the full 3D problem. However here, a 2D approach is sufficient to explore the practicalities of joint inversion.

The two components of apparent resistivity are denoted $\tilde{\rho}_{TE}$ and $\tilde{\rho}_{TM}$ and they vary with frequency, ω. For the 2D resistivity distribution, $\rho(y,z)$, components of $\tilde{\rho}(y,\omega)$ at surface locations, y, are computed using the ModEM code (Modular system for Electromagnetic inversion; Kelbert et al., 2014) operating in forward mode. To minimise boundary effects, the 2D distribution $\rho(y,z)$ abstracted directly from the alteration model $\Gamma(T; \boldsymbol{\theta})$ is embedded within a larger grid that extends to a depth of 80 km and 70 km either side of the geothermal system. This grid is vertically stratified with the following resistivity properties: (i) TVZ surface fill – 200 Ωm to a depth of 2 km, (ii) greywacke basement – 1000 Ωm to a depth of 8 km, and (iii) upper crust – 200 Ωm to a depth of 80 km.

Fig. 4 shows $\tilde{\rho}_{TE}$ and $\tilde{\rho}_{TM}$ as a function of station location and frequency above the geothermal system with resistivity shown in Fig. 3B. As $\tilde{\rho}$ is obtained directly from ρ, we refer to it as the "true" apparent resistivity. This step corresponds to the arrow labeled ② in Fig. 1.

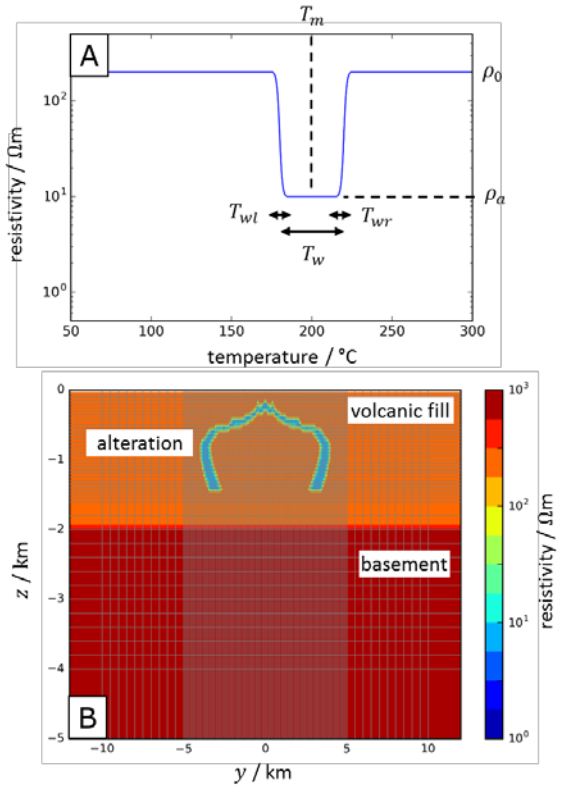

Figure 3: Summary of clay alteration model. A. Box-car function, $\Gamma(\cdot)$, prescribing electrical resistivity in terms of equilibrium geothermal temperature. Function parameters are explained in Section 2.2. B. "True" resistivity distribution, $\rho(y,z)$, when the alteration model in A is applied to the temperature distribution in Fig. 2A. The low resistivity "clay cap" is indicated by the blue halo.

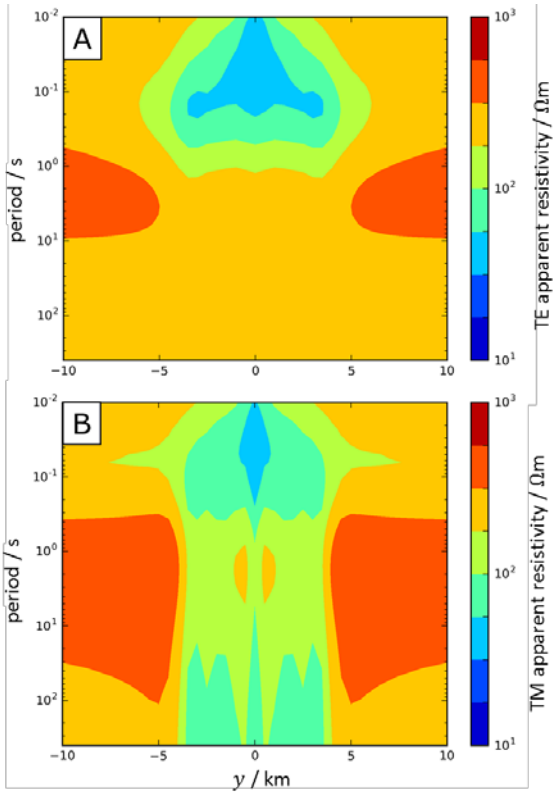

Figure 4: Components of apparent resistivity, $\tilde{\rho}(y,\omega)$, obtained from the forward MT model applied to the distribution in Fig. 3B. These fields are sampled to yield the MT survey observations, $\tilde{\rho}_{obs}$.

3. JOINT INVERSION METHODOLOGY

The goal of joint inversion is to infer a subsurface temperature distribution from an MT survey and downhole temperature measurements. For the synthetic model analysed here, there are three steps to the inversion:

1. Extract "observations" of temperature and apparent resistivity by sampling from the synthetic model.
2. Invert apparent resistivity to obtain an inferred distribution of subsurface resistivity.
3. Model how "observed" temperature relates to inferred resistivity at the well and extrapolate this relationship away from the borehole to obtain an inferred temperature distribution.

Each of these steps is expanded on below.

3.1 Observations

The join inversion methodology applied here requires two sources of data: (1) downhole temperature measurements in thermally equilibrated geothermal wells, and (2) surface measurements of apparent resistivity obtained by an MT survey. As this is a proof-of-concept study, it is sufficient to obtain both these datasets from the synthetic model, i.e., by directly sampling $T(y,z)$ and $\tilde{\rho}(y,\omega)$. For a vertical well at horizontal position, y_w, and for MT surface stations at locations, y_s, and with bandwidth, ω_s, the "observations" are denoted $T_{obs} = T(y_w, z)$ and $\tilde{\rho}_{obs} = \tilde{\rho}(y_s, \omega_s)$.

For this analysis, we have supposed there is a well situated in the centre of the upflow zone ($y_w = 50$ m) and that equilibrated temperatures have been measured to a depth of 1 km. For the MT survey, we have used a station spacing of 500 m out to 10 km from the centre of the upflow and a bandwidth of 0.01 to 400 seconds.

The observation steps correspond to the arrows labelled ③ and ④ in Fig. 1.

3.2 Inversion for resistivity

ModEM, the code used in the forward model in step ② to obtain $\tilde{\rho}(y,\omega)$ from $\rho(y,z)$, is principally an inversion code designed to infer subsurface distributions of electrical resistivity. For the synthetic MT survey observations, $\tilde{\rho}_{obs}$, we use ModEM to invert for a subsurface resistivity distribution, $\rho'(y,z)$.

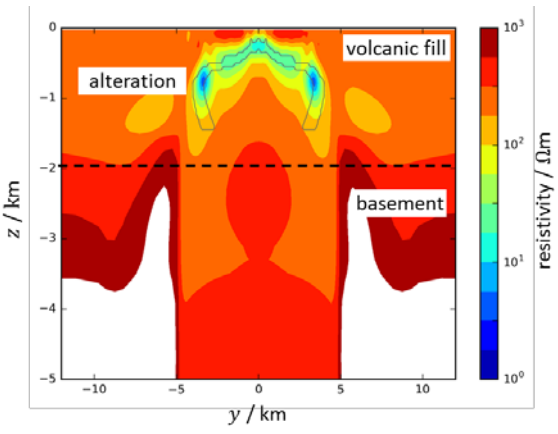

Figure 5: Inferred resistivity distribution, $\rho'(y,z)$, obtained by inversion of the MT observations $\tilde{\rho}_{obs}$. The dashed line indicates the depth of the basement where there is a resistivity contrast. An outline of the clay alteration zone in Fig. 3B has been superimposed.

Such inversions are typically ill-posed problems and some form of regularization is necessary to obtain a unique solution. As a result, the inferred distribution, ρ', is not likely to match the "true" distribution, ρ. This is particularly true when there are sharp boundaries in the distribution of ρ; the regularization algorithm will tend to smooth these out.

ModEM, used in inverse mode, was applied to the observations $\tilde{\rho}_{obs}$ to obtain the inferred resistivity distribution, ρ', shown in Fig. 5. While the smoothing effects of the regularization are apparent, the inversion nevertheless captures the size, shape and resistivity properties of the clay cap formed above the upflow zone (see true cap structure, overlaid as a black contour).

The inversion for resistivity corresponds to step ⑤ in Fig. 1.

3.3 Joint inversion for temperature

A perfect inversion of ρ' from $\tilde{\rho}_{obs}$ would return the "true" resistivity distribution, ρ. From this, and assuming we knew parameters of the alteration model, $\mathbf{\theta}$, we might infer aspects of the distribution T by applying the inverse transformation $T = \Gamma^{-1}(\rho; \mathbf{\theta})$ (of course, this would still be hampered by the non-monotonicity of Γ).

In practice, the inferred ρ' is an imperfect approximation of the "true" ρ. Furthermore, we have little knowledge of the alteration model, $\Gamma(T; \mathbf{\theta})$, except perhaps a qualitative sense of its functional form and parameter values (e.g., we might "understand" that alteration to a resistivity value, ρ_a, occurs dominantly in the interval $[T_{min}, T_{max}]$). However, by comparing values of ρ' sampled along the well track, denoted ρ'_{well}, to the corresponding temperatures, T_{obs}, we can begin to build a quantitative (if empirical) model linking T and ρ'.

Fig. 6A compares ρ'_{well} and T_{obs} for the case investigated here, a well in the centre of the upflow. Once more, the smoothing effect of regularization in the inversion for ρ' is apparent. In this case, $\log(\rho'_{well})$ is reasonably well approximated by a normal distribution function with a mean at $z = 270$ m and a standard deviation of 120 m.

The temperature profile has the characteristic convective shape (steep gradient at depth, shallowing as it approaches the surface) and we have elected to approximate its shape with a simple 1D heat transport model developed by Bredehoeft and Papadopoulos (1965)

$$T = (T_{max} - T_{min}) \frac{\exp\left(\beta \frac{z - z_{min}}{z_{max} - z_{min}}\right) - 1}{\exp(\beta) - 1} + T_{min},$$

where $[z_{min}, T_{min}]$ and $[z_{max}, T_{max}]$ are boundary conditions and β captures the relative strength of conductive versus convective heat transfer. This model is expressed $T = f(z; \mathbf{\phi})$ where $\mathbf{\phi} = [\beta, z_{min}, z_{max}, T_{min}, T_{max}]$ is a vector of model parameters. Fixing T_{min}= 25°C and T_{max}= 300°C, we obtain a best fit to T_{obs} when β = -4.0, z_{min} = 170 m and z_{max}= 1810 m.

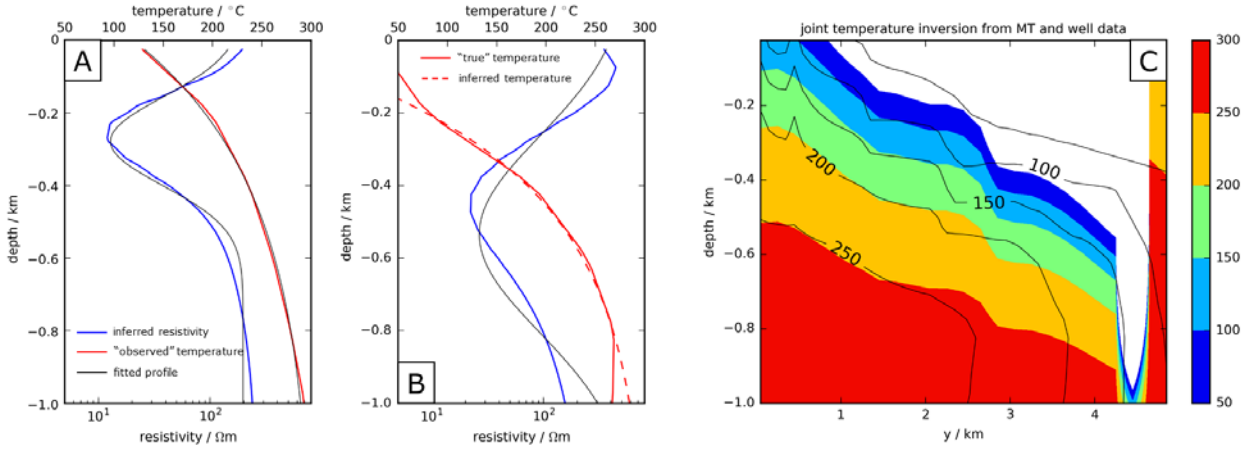

Figure 6: Summary of joint inversion. A. Temperature measurements, T_{obs} (red line) and corresponding values of ρ' (blue) for a well located in the centre of the upflow. Function fits (described in the text) are indicated by black lines. B. For a vertical profile at y = 1.5 km, values of ρ' (blue line), best-fit normal distribution (black), inferred temperature (red dashed) extrapolated from the correlation in A and the "true" temperature (red solid). C. Comparison between inferred, $T'(y,z)$ (filled contours) and "true" temperature distribution (black isotherms).

Having expressed ρ'_{well} and T_{obs} as functions of depth, we have effectively developed a semi-empirical model that correlates notable features of the vertical profile ρ'_{well} (e.g., the centre of mass of the best-fit normal distribution) to a particular value of in situ temperature. A simple means of extrapolating this correlation to another vertical profile not coincident with the well, say ρ'_i situated at y_i, would be to: (i) find the centre of mass of the best-fit normal distribution to ρ'_i, (ii) identify how the depth of this centre is offset compared to that for ρ'_{well}, and (iii) translate the profile T_{obs} upward or downward accordingly, yielding T'_i. This simple approach implicitly assumes that the model calibrated for 1D heat transport at T_{obs} is a good representation of heat transport throughout the upflow zone (i.e., all possible y_i). Fig. 6B plots ρ'_i and T'_i for a vertical profile offset 1.5 km horizontally from the well. Despite the normal distribution being a relatively poor approximation to the profile ρ'_i, the agreement between the inferred and "true" temperature profile is nevertheless quite good.

Extrapolation of the model correlating T_{obs} to ρ'_{well} has been applied over the upper 1 km of the geothermal system and out to a distance of 5 km from the centre of the upflow. This extends slightly beyond the clay cap (Fig. 3B). The resulting inferred temperature distribution, $T'(y,z)$, is shown by the coloured contours in Fig. 6C.

The joint inversion described in this section corresponds to the step labelled ⑥ in Fig. 1.

3.4 Validation

The effectiveness of joint inversion on this synthetic example is evaluated by a direct comparison between T and T', the "true" and inferred temperature distributions. Fig. 6C shows that agreement in the temperature range 100 to 250°C is quite reasonable out to a distance of nearly 3 km from the centre of the upflow. At distances larger than 4 km, the clay cap becomes more vertically oriented (aligning with the 200°C isotherm, which also starts to tilt downward), its signature in the inferred resistivity distribution becomes more smeared in the vertical and, as a result, agreement between T and T' is substantially worsened.

Validation is labelled as step ⑦ in Fig. 1.

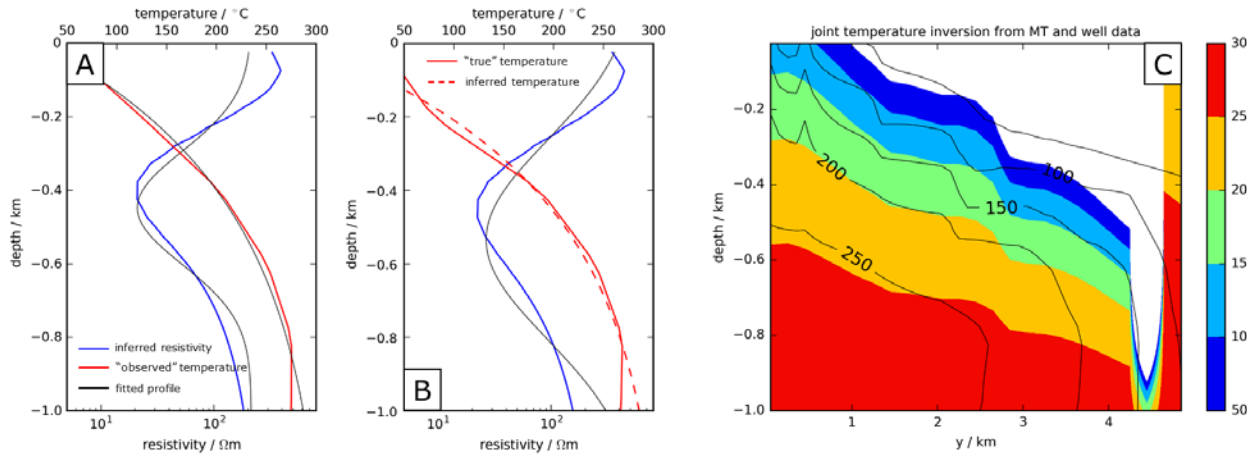

Figure 7: Joint inversion of temperature distribution using temperatures in a well centred at y_w= 1.0 km (c.f. Fig. 6, a well centred at y_w= 0).

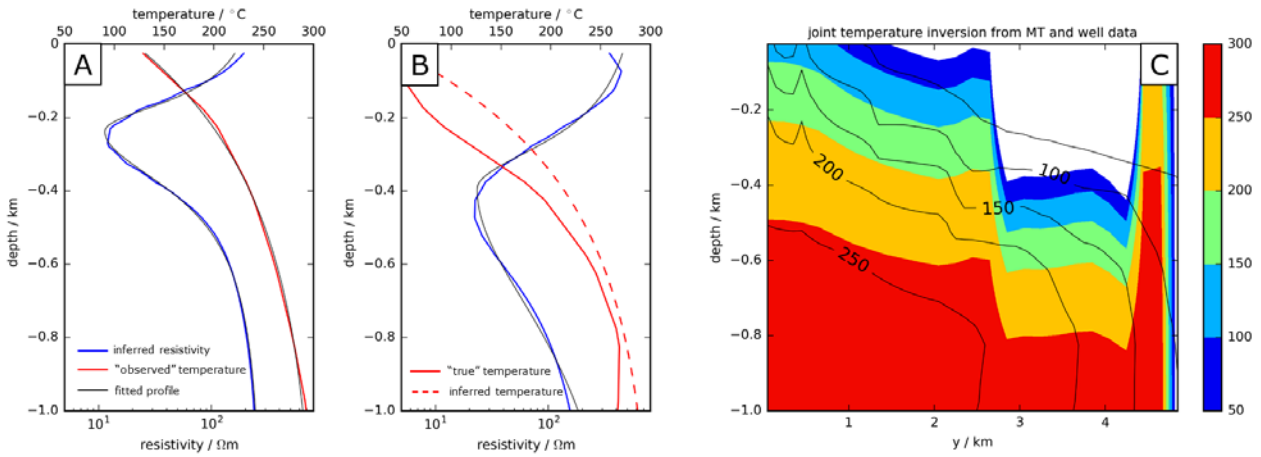

Figure 8: Joint inversion of temperature distribution when an asymmetric Cauchy distribution is used to fit the resistivity profiles in A and B (blue). In spite of the improved fit, the resulting temperature inversion does not agree as well with the "true" distribution.

4. VARIATIONS ON THE INVERSION

We have investigated a few variations on this joint inversion approach that affect the final accuracy.

In practice, well data might only be available at some lateral offset, rather than in the centre of the upflow zone. Fig. 7 shows the result of the joint inversion using a well that is offset 1 km from the upflow centre. The match between inferred and "true" temperature distributions is of a similar quality to that in Fig. 6. This appears to be a general result for wells that intersect the clay cap (i.e., within ~3 km of the centre of the upflow).

We have also considered alterative functions that provide an better fit to the shape of $\log(\rho'_{well})$. One such class of functions is an asymmetric Cauchy distribution function, which is better at capturing the heavy tails in the data

$$\rho'_{well} = \rho_0 - A\left[1 + \left(\frac{z-\mu_z}{\gamma_i}\right)^2\right]^{-1},$$

where μ_z is the depth of the function minimum and the two scale factors describing behaviour above and below this depth are $\gamma_i = \gamma_u$ for $z > \mu_z$ and γ_l for $z \leq \mu_z$. This functional form provides a good fit to the profiles in Fig. 8A and B. As in Fig. 6 and 7, the relative offset in μ_z between profiles of ρ'_{well} and ρ' is used to extrapolate an inferred distribution T'. In spite of the improved fit to ρ'_i by the Cauchy function, the agreement between T and T' (Fig. 8C) is worse than when using the normal distribution fit.

5. FUTURE IMPROVEMENTS

The joint inversion study described above contains a number of limitations that could be addressed in future studies:

1. We have not accounted for sources of uncertainty in the MT observations. ModEM provides for specification of errors in the $\tilde{\rho}$ measurements used to perform the inversion. Other studies typically set these on the order of 5 to 10% (e.g., Heise et al., 2008; Bertrand et al., 2012).
2. Often, temperature data are available from more than one well. In this case, the joint inversion needs to consider how the correlation model should be developed when there is more than one coincident pair of (T_{obs}, ρ'_{well}). This is a similar problem to that explored by Muñoz et al. (2010) who investigated correlation structures between seismic velocity and resistivity.
3. The MT inversion in this study assumed a 2D Earth with no change in properties in the out-of-plane dimension. However, real geothermal fields are localised features in 3D space and thus 3D effects are likely to be important. Resolving out-of-plane features requires additional MT station coverage as well as greater computational resources to perform the inversion for resistivity.
4. We have only considered one "true" alteration model, $\Gamma(\cdot)$, whose parameters were based on a review of the literature. The "true" alteration model (and therefore the clay cap geometry) is likely to be site dependent. Different alteration models, $\Gamma_i(\cdot)$, may produce clay caps for which joint inversion is more or less accurate across particular temperature ranges.
5. Ultimately, the usefulness of this joint inversion approach will be best assessed through application to a real site. The ideal candidate would be a well-developed field with abundant well data, a recent MT survey and a well-calibrated reservoir model, all of which would aid in validating the inferred temperature distribution, T', and the inversion algorithm.

ACKNOWLEDGEMENTS

The authors are grateful to Gary Egbert for providing access to the ModEM code used in this study.

REFERENCES

Bertrand, E. A., T. G. Caldwell, G. J. Hill, E. L. Wallin, S. L. Bennie, N. Cozens, S. A. Onacha, G. A. Ryan, C. Water, A. Zaino, and P. Wameyo: Magnetotelluric imaging of upper-crustal convection plumes beneath

the Taupo Volcanic Zone, New Zealand. *Geophys. Res. Lett.* 39, doi: 10.1029/2011GL050177. (2012).

Bredehoeft, J. D., and I. S. Papadopulos: Rates of Vertical Groundwater Movement Estimated from the Earth's Thermal Profile. *Water Res. Res.*, 1, pp. 325-328. (1965).

Heise, W., T. G. Caldwell, H. M. Bibby, and S. C. Bannister: Three-dimensional modelling of magnetotelluric data from the Rotokawa geothermal field, Taupo Volcanic Zone, New Zealand. *Geophys. J. Int.* 173, pp. 740-750. (2008).

Kelbert, A., N. Meqbel, G. D. Egbert, and K. Tandon: ModEM: A modular system for inversion of electromagnetic geophysical data. *Comp. Geosci.* 66, pp. 40-53. (2014).

Mellors, R. J., A. Tompson, X. Yang, M. Chen, A. Ramirez, and J. Wagoner: Stochastic Joint Inversion Modeling Algorithm of Geothermal Prospects. Proc. 40th Workshop on Geothermal Reservoir Engineering, Stanford, CA, USA. (2015).

Morrison, K.: Important hydrothermal minerals and their significance. *Geothermal and Mineral Service Div., Kingston Morrison Ltd.* (1997).

Muñoz, G., K. Bauer, I. Moeck, A. Schulze, and O. Ritter: Exploring the Groß Schönebeck (Germany) geothermal site using a statistical joint interpretation of magnetotelluric and seismic tomography models. *Geothermics* 39, pp. 35-45. (2010).

O'Sullivan, J., and M. O'Sullivan: The Effect of Bottom Boundary Conditions on Predictions of Steam Production from Geothermal Reservoir Models. Proc. 41st Workshop on Geothermal Reservoir Engineering, Stanford, CA, USA. (2016).